

Quantum Phase Transitions in Superconducting Arrays with General Capacitance Matrices

Beom Jun Kim, Jeenu Kim, Sung Yong Park, and M.Y. Choi
*Department of Physics and Center for Theoretical Physics
Seoul National University
Seoul 151-742, Korea*

We investigate quantum phase transitions in two-dimensional superconducting arrays with general capacitance matrices and discrete charge states. We use the perturbation theory together with the simulated annealing method to obtain the zero-temperature phase diagrams, which display various lobe-like structures of insulating solid phases, and examine the possibility of supersolid phase. At nonzero temperatures, an effective classical Hamiltonian is obtained through the use of the variational method in the path-integral formalism, and the corresponding phase diagram is found approximately. The insulating lobes of the solid phases are shown to exist at sufficiently low temperatures, and results of Monte Carlo simulations are also presented.

PACS numbers: 74.50.+r, 67.40.Db, 05.30.Jp

I. INTRODUCTION

Two-dimensional (2D) superconducting arrays, weakly coupled by Josephson junctions, have attracted much attention [1]. In the classical array, where the charging energy is neglected, the relevant variable is the phase of the superconducting order parameter at each grain, and the logarithmic interaction between vortices is well known to lead to the Berezinskii-Kosterlitz-Thouless (BKT) transition [2]. Recent development of the fabrication techniques, on the other hand, allows to make regular arrays composed of very small superconducting grains. In such arrays the charging energy cannot be neglected any longer [3], and studies considering both the self-capacitance C_0 and the junction capacitance C_1 are required. In the presence of Ohmic dissipation, the charges, which are conjugate to the phase variables, take continuous values and the corresponding phase diagrams have been obtained through the use of a variational method [4]. This has revealed the existence of a low-temperature reentrant transition, which appears consistent with the recent quantum Monte Carlo study [5]. Without dissipation, in contrast, the charges change in discrete quanta $2e$ with $-e$ being the electron charge. In this case the phase diagrams have been investigated via the coarse-graining approximation, which is mean-field-like in nature [6]. In general, the mean-field approximation does not give reliable results in two dimensions, where fluctuations are too strong to be neglected. It is thus desirable to study the 2D superconducting arrays, with general capacitance matrices and discrete charge states, beyond the mean-field approximation.

The quantum phase transitions in the superconducting arrays have drawn much interest also in relation to the Bose-Hubbard model, which describes strongly interacting bosons under the competition between the kinetic-energy and the potential-energy effects. Here the ki-

netic energy and the potential energy correspond to the Josephson energy and the charging energy in the superconducting array, respectively. In the presence of the on-site potential, the system at zero temperature exhibits a transition between the Mott insulating phase and the superfluid phase, displaying lobe-like structures in the resulting phase diagram [7,8]. In addition, nearest-neighbor interactions and next nearest-neighbor interactions produce various phases such as the checker-board-type solid, the striped solid, and the supersolid. In particular, the supersolid phase, which is characterized by superfluidity in the presence of underlying commensurability, has been studied extensively [9,10].

This paper investigates the phase transitions in 2D superconducting arrays with emphasis on the effects of charge frustration and on the competition between the self- and junction capacitances. At zero temperature, we use the perturbation expansion and the simulated annealing method to obtain various insulating lobes. Here rational charge frustration introduces commensurability effects to the array, leading to the solid phases with various charge densities. The detailed phase boundaries depend crucially on the ratio of the junction to self-capacitances, C_1/C_0 : For example, the insulating lobes become narrower and their central positions approach the charge frustration values, as C_1/C_0 is increased. Further, as the system size is increased, more and more insulating lobes are expected to be observed in the phase diagram, suggesting the interesting possibility of the lobe at every rational frustration in the thermodynamic limit. To check the robustness of the lobes against finite temperatures, we apply the Monte Carlo (MC) method to the system without the Josephson term and find the persistence of the insulating lobes with low-order rational values of the charge density. We also use a variational method to obtain an effective classical Hamiltonian describing the system at finite temperatures. The corresponding phase di-

agrams are found approximately in a self-consistent manner, which again display lobes with the half-filled charge density. In the absence of charge frustration, the effective classical Hamiltonian has only real terms, which allows us to use the MC method: We obtain the critical strengths of the Josephson coupling and compare them with ones obtained from the self-consistent approximation. In the self-charging limit, the possibility of a reentrant transition is also pointed out.

This paper is organized as follows: Section II introduces the quantum mechanical Hamiltonian for the superconducting arrays with general capacitance matrices and discrete charge states. Such a superconducting array is described by quantum mechanical conjugate variables, charges and phases, and charge frustration is induced by applying an external voltage between the array and the substrate. In Sec. III, we study the zero-temperature phase transitions in the system via the perturbation expansion together with the simulated annealing method. The phase transitions at vanishing charge density is investigated in Sec. III A, where the results in the nearest-neighbor charging limit are also compared with those of the previous works. In Sec. III B, phase transitions at finite charge densities are studied, and

the nature as well as the existence of the supersolid phase is discussed. Section IV is devoted to the investigation of the finite-temperature phase transitions by means of a variational method and MC simulations. The system without the Josephson coupling is described by only charge variables, and we present the corresponding MC results in Sec. IV A, where the charge densities are obtained as functions of the charge frustration at various temperatures. The resulting step structures at zero temperature are compared with those obtained in Sec. III B. Whereas the phase diagrams in the presence of the Josephson coupling are obtained in a self-consistent manner in Sec. IV B, the comparison with MC results reveals that the self-consistent approximation is accurate only at sufficiently high temperatures. Finally, a summary of the paper is given in Sec. V.

II. MODEL HAMILTONIAN

We consider an $L \times L$ ($N \equiv L^2$) square array of Josephson junctions. The extra charge Q_i on the superconducting grain at site i can be written as

$$\begin{aligned} Q_i &= C_0 \Phi_i + C_1 (\Phi_i - \Phi_{i+\hat{x}}) + C_1 (\Phi_i - \Phi_{i-\hat{x}}) + C_1 (\Phi_i - \Phi_{i+\hat{y}}) + C_1 (\Phi_i - \Phi_{i-\hat{y}}) \\ &\equiv \sum_j C_{ij} \Phi_j, \end{aligned} \quad (1)$$

where C_0 and C_1 are the self- and the junction capacitances, respectively, and Φ_i is the electric potential of the grain i with respect to the substrate. If we apply an external voltage Φ_x between the substrate and the ground, Eq. (1) is changed to $Q_i = \sum_j C_{ij} \Phi_j + Q_x$, with the ‘‘gauge charge’’ $Q_x \equiv C_0 \Phi_x$. The Hamiltonian describing such a superconducting array consists of two parts:

$$\begin{aligned} H &= H_0 + V \\ &= \frac{1}{2} \sum_{i,j} (Q_i - Q_x) C_{ij}^{-1} (Q_j - Q_x) - E_J \sum_{\langle i,j \rangle} \cos(\phi_i - \phi_j), \end{aligned} \quad (2)$$

where ϕ_i represents the phase of the superconducting order parameter at site i . Note that the charge Q_i and the phase ϕ_i are quantum mechanical conjugate variables satisfying the commutation relation $[\phi_i, Q_i] = 2ei$ ($e > 0$). In the charging energy term H_0 , the charges at sites i and j interact via the inverse of the capacitance matrix C_{ij}^{-1} whereas the summation in the Josephson energy term V is to be done over all the nearest neighboring pairs. When the lattice constant of the array approaches zero, we can write Eq. (1) in the continuum form $Q(\mathbf{r}) = C_0 \Phi(\mathbf{r}) - C_1 \nabla^2 \Phi(\mathbf{r})$ and obtain $\Phi(\mathbf{r})$ due to a single positive charge at the origin [11]: $\Phi(\mathbf{r}) \propto K_0(r/\Lambda)$ with the modified Bessel function K_0 , where the screening length Λ ($\equiv \sqrt{C_1/C_0}$) measures the interaction range between charges. The above Hamiltonian in Eq. (2) is

closely related to the Bose-Hubbard Hamiltonian and to the spin-1/2 XXZ Hamiltonian [10]. The charging energy term in Eq. (2) drives the system to arrange its discrete charges such that the average charge per site is as close to Q_x as possible, and the Josephson energy corresponds to the hopping energy in the Bose-Hubbard model [12]. Consequently, if the charging energy is sufficiently larger than the Josephson energy, hopping is suppressed and all the charges are arranged to form a periodic lattice, leading to the insulating phase at zero temperature. In particular, when $E_J = 0$, the energy eigenstate can be chosen also as a simultaneous eigenstate of the charge operator since $[Q_i, H] = 0$. The uncertainty relation between the charge and the phase then asserts that phase coherence and consequently, superconductiv-

ity cannot be attained in this limit. In the opposite limit of the strong Josephson coupling, all the charges are in the extended state owing to the dominant hopping term,

and the superconducting phase is favored. For convenience, we write $q_i \equiv Q_i/2e$, $q_x \equiv Q_x/2e$, $E_0 \equiv e^2/2C_0$, and $\tilde{C}_{ij} \equiv C_{ij}/C_0$, and obtain Eq. (2) in the form

$$H = H_0 + V = 4E_0 \sum_{i,j} (q_i - q_x) \tilde{C}_{ij}^{-1} (q_j - q_x) - E_J \sum_{\langle i,j \rangle} \cos(\phi_i - \phi_j), \quad (3)$$

where the inverse of the dimensionless capacitance matrix is given by

$$\tilde{C}_{ij}^{-1} = \frac{1}{N} \sum_{\mathbf{k}} \frac{e^{i\mathbf{k}\cdot(\mathbf{x}_i - \mathbf{x}_j)}}{1 + 4C_1/C_0 - 2(C_1/C_0)(\cos k_x + \cos k_y)}. \quad (4)$$

III. ZERO-TEMPERATURE PHASE DIAGRAMS

In general the state which minimizes the energy determines the zero-temperature phase of the system. Suppose that we have obtained the energy levels of the system which correspond to the ground state, the first excited state, etc. If we introduce a small change in the control parameters, the energy levels shift by a small amount, and it is possible that the ground state and the first excited state cross each other as we pass through a set of values of the control parameters; this “level crossing” leads to a zero-temperature phase transition in the parameter space [13]. It should be noted here that consideration of only the two low-lying states, the ground state and the first excited one, may not be sufficient. Figure 1 shows schematic dependence of the energy levels E_n on the control parameter K in two possible cases. In Fig. 1 (a), the ground state and the first excited state cross at the critical value K_1 of the control parameter, which corresponds to the true transition point. In Fig. 1 (b), on the other hand, the true transition point is given by K_2 , where the ground state and the second excited one cross each other. In this case consideration of only the two low-lying states would lead to K_1 , which is not the true transition point. To find the true transition point, we thus need to consider all the energy levels, which is not possible in practice. Despite this, considering the level crossing of the ground state and the first excited state is very useful and convenient to obtain the upper limit of the true transition point.

In terms of charges the system can be either in the incommensurate conducting phase or in the commensurate insulating phase; in the latter charges are expected to form a superlattice which covers periodically the whole system. If the commensurate state has energy lower/higher than that of the incommensurate state for given values of parameters, the system should be in the insulating/conducting phase. (Here E_J/E_0 , q_x , and C_1/C_0 constitute the control parameters.) Accordingly, for given total number of charges, it is needed to find the charge configurations of the commensurate state and of the low-lying incommensurate states. The symmetry of the Hamiltonian under the transformations

$$\begin{cases} q_x \rightarrow q_x + 1, \\ q_x \rightarrow -q_x, \end{cases} \quad (5)$$

allows us to consider q_x only in the range $0 \leq q_x < 1/2$. In this restricted range $0 \leq q_x < 1/2$, the commensurate states of the system may be classified in terms of the average number of charges, $\langle q_i \rangle \equiv \sum_i q_i/N$. For $\langle q_i \rangle = p/q$ with relatively prime integers p and q , the charges are expected to form a $q \times q$ superlattice, on the unit cell of which pq charges, each with the unit charge, are located.

A. Phase transitions for $\langle q_i \rangle = 0$

We first investigate the phase transitions in the system with $\langle q_i \rangle = 0$. The energy of the $\langle q_i \rangle = 0$ commensurate state is computed via the second-order perturbation expansion with the Josephson term as a perturbation in Eq. (3), and is written as

$$E_{(c)}(\langle q_i \rangle = 0) = E_{(c)}^{(0)}(0) + E_{(c)}^{(1)}(0) + E_{(c)}^{(2)}(0) + O(E_J^3). \quad (6)$$

Without the perturbation, the Hamiltonian of the system contains only charge operators and yields the eigenfunction

$$\langle \phi | \mathbf{q} \rangle \equiv \langle \phi_1, \phi_2, \phi_3, \dots, \phi_N | q_1, q_2, q_3, \dots, q_N \rangle = \left(\frac{1}{\sqrt{2\pi}} \right)^N \exp \left(i \sum_i q_i \phi_i \right), \quad (7)$$

which is simply the plane-wave state of the usual free particle system, with the interpretation of ϕ_i and q_i as the position and the momentum, respectively. For the commensurate state with $\langle q_i \rangle = 0$, all the charge eigenvalues q_i 's are zero and it is easy to compute the zeroth-order contribution $E_{(c)}^{(0)}(0)$ and the first-order contribution $E_{(c)}^{(1)}(0)$: $E_{(c)}^{(0)}(0) = 4E_0 q_x^2 \sum_{i,j} \tilde{C}_{ij}^{-1} = 4E_0 q_x^2 N$ and $E_{(c)}^{(1)}(0) = \langle \mathbf{q} = 0 | V | \mathbf{q} = 0 \rangle = (1/2\pi)^N \int (\prod_i d\phi_i)$

$\sum_{\langle i,j \rangle} \cos(\phi_i - \phi_j) = 0$. The second-order contribution is given by

$$E_c^{(2)}(0) = \sum_{\mathbf{q}' \neq 0} \frac{|\langle \mathbf{q}' | V | \mathbf{q} = 0 \rangle|^2}{E^{(0)}(\mathbf{q} = 0) - E^{(0)}(\mathbf{q}')}, \quad (8)$$

where $E^{(0)}(\mathbf{q})$ is the zeroth-order energy for the charge configuration \mathbf{q} , and

$$\begin{aligned} \langle \mathbf{q}' | V | \mathbf{q} = 0 \rangle &= \langle \mathbf{q}' | -E_J \sum_{\langle i,j \rangle} \cos(\phi_i - \phi_j) | \mathbf{q} = 0 \rangle \\ &= -\frac{E_J}{2(2\pi)^N} \sum_{\langle i,j \rangle} \int \prod_k d\phi_k \left[e^{i(\phi_i - \phi_j - \sum_k q'_k \phi_k)} + e^{i(\phi_j - \phi_i - \sum_k q'_k \phi_k)} \right] \\ &= -\frac{E_J}{2} \sum_{\langle i,j \rangle} \left[\prod_{k \neq i,j} \delta(q'_k, 0) \right] [\delta(q'_i, 1)\delta(q'_j, -1) + \delta(q'_j, 1)\delta(q'_i, -1)]. \end{aligned} \quad (9)$$

Inserting Eq. (9) into Eq. (8), we obtain the energy of the $\langle q_i \rangle = 0$ commensurate state to the 2nd order in E_J :

$$E_{(c)}(0) \approx 4E_0 N q_x^2 - \frac{E_J^2 N}{8E_0 (\tilde{C}_{00}^{-1} - \tilde{C}_{10}^{-1})}. \quad (10)$$

We next consider the incommensurate state with $\langle q_i \rangle = 0$. Among the various excitations present in the system with the constraint $\langle q_i \rangle = 0$, the lowest excitation is expected to be point-like and we consider two types of excitations: One is the creation of a single charge (SC) at one site [8], and the other is the creation of a charge dipole (CD) at one bond [$q_i = 1, q_j = -1$ with (i, j) being the nearest-neighboring pair]. Both excitations do not change the value of $\langle q_i \rangle$ in the thermodynamic limit ($N \rightarrow \infty$). In the self-charging limit ($C_1 = 0$), the interaction matrix C_{ij}^{-1} takes a diagonal form and the first excited state should be of the SC type, since the CD type excitation requires the creation energy of

two charges. On the other hand, in the nearest-neighbor (NN) charging limit ($C_0 = 0$), only the excitations which does not change the total number of charges are allowed and the first excited state is expected to be of the CD type. Accordingly, as the value of C_1/C_0 is increased, the first excited state should change from the SC type to the CD type at a critical value of C_1/C_0 . In particular, the system in the NN charging limit displays the charge-anticharge unbinding transition [11,14,15], the BKT nature of which is manifested by the square-root cusp in the resistance [15]. This charge BKT transition is suppressed by the presence of the self-capacitance, making the screening length finite, and it seems likely that the change of the first excited state according to the value of C_1/C_0 in turn leads to the change in the nature of the transition.

Between the above two types of excitations, the lowest one is determined from the comparison of the zeroth-order energies of both types: If ΔE given by

$$\begin{aligned} \Delta E &\equiv E^{(0)}(\text{SC}) - E^{(0)}(\text{CD}) \\ &= 4E_0 (\tilde{C}_{00}^{-1} - 2q_x + Nq_x^2) - 4E_0 (\tilde{C}_{00}^{-1} - \tilde{C}_{01}^{-1} - \tilde{C}_{10}^{-1} + \tilde{C}_{11}^{-1} + Nq_x^2) \\ &= 4E_0 (2\tilde{C}_{10}^{-1} - \tilde{C}_{00}^{-1} - 2q_x) \end{aligned} \quad (11)$$

is negative/positive, the creation of a single charge/charge dipole is the lowest excitation. Figure 2 shows the boundary for $\Delta E = 0$ in the limit of $N \rightarrow \infty$. It is found that for $C_1/C_0 < 14.116$ the lowest excitation is of the SC type regardless of the value of q_x , and that the region of the CD type excitation (the region below the curve in Fig. 2) is quite small, allowed only for $q_x < 9.4 \times 10^{-4}$. Therefore we below focus on the SC type excitation for $C_0 \neq 0$ and $q_x > 0$, and then consider the CD type excitation only in the NN charging limit ($C_0 = 0$) with $q_x = 0$.

We write the energy of the first excited state of the SC type as

$$E_{(ic)}(\langle q_i \rangle = 0) = E_{(ic)}^{(0)}(0) + E_{(ic)}^{(1)}(0) + E_{(ic)}^{(2)}(0) + O(E_J^3), \quad (12)$$

and the eigenstate as

$$|\mathbf{q}^{(l)}\rangle = |q_1^{(l)}, q_2^{(l)}, \dots, q_N^{(l)}\rangle \quad \text{with} \quad \begin{cases} q_i^{(l)} = 1 & \text{for } i = l, \\ q_i^{(l)} = 0 & \text{otherwise,} \end{cases} \quad (13)$$

which is expected to be a superconducting state since the extra charge at site l can hop to any site without energy cost. Inserting Eq. (13) to H_0 in Eq. (3), we obtain the zeroth-order contribution: $E_{(ic)}^{(0)}(0) = 4E_0(\tilde{C}_{00}^{-1} - 2q_x + Nq_x^2)$, where we have used the translational symmetry $\tilde{C}_{ll}^{-1} = \tilde{C}_{00}^{-1}$ and $\sum_j \tilde{C}_{ij}^{-1} = 1$. Since the above excited state in Eq. (13) has an N -fold degeneracy (l can take values $1, 2, \dots, N$), we use the degenerate perturbation theory to calculate the first-order contribution $E_{(ic)}^{(1)}(0)$. We thus need to diagonalize the matrix V whose components are given by

$$\begin{aligned} V_{lm} &\equiv \langle \mathbf{q}^{(l)} | V | \mathbf{q}^{(m)} \rangle \\ &= \begin{cases} -E_J/2 & \text{for } (l, m) \text{ nearest neighboring pair,} \\ 0 & \text{otherwise.} \end{cases} \end{aligned} \quad (14)$$

For that purpose, it is convenient to use the Fourier transform:

$$V_{lm} = \frac{1}{N} \sum_{\mathbf{k}} e^{i\mathbf{k} \cdot (\mathbf{x}_l - \mathbf{x}_m)} \tilde{V}_{\mathbf{k}}, \quad (15)$$

which gives straightforwardly the eigenvalues $\tilde{V}_{\mathbf{k}} = -E_J(\cos k_x + \cos k_y)$. The first-order contribution is then given by the lowest eigenvalue: $E_{(ic)}^{(1)}(0) = \tilde{V}_{\mathbf{k}=0} = -2E_J$. For this lowest-lying excited state with $\mathbf{k} = 0$, it is also straightforward to obtain the second-order contribution, which leads to the energy of the incommensurate state

$$\begin{aligned} E_{(ic)}(0) &\approx 4E_0(Nq_x^2 - 2q_x + \tilde{C}_{00}^{-1}) - 2E_J + \frac{E_J^2}{32E_0} \sum'_{(i,j)} \frac{1}{\tilde{C}_{j0}^{-1} - \tilde{C}_{i0}^{-1} - \tilde{C}_{00}^{-1} + \tilde{C}_{10}^{-1}} \\ &+ \frac{E_J^2}{8E_0} \left(\frac{2}{\tilde{C}_{10}^{-1} - \tilde{C}_{\hat{x}+\hat{y},0}^{-1} - \tilde{C}_{00}^{-1} + \tilde{C}_{10}^{-1}} + \frac{1}{\tilde{C}_{10}^{-1} - \tilde{C}_{2\hat{x},0}^{-1} - \tilde{C}_{00}^{-1} + \tilde{C}_{10}^{-1}} \right). \end{aligned} \quad (16)$$

Here $\sum'_{(i,j)}$ denotes the summation over i and its four nearest-neighbors j with the restriction $j \neq 0$. The zero-temperature transition occurs when the energy of the commensurate state given by Eq. (10) and that of the incommensurate state given by Eq. (16) becomes equal. This reveals the zero-temperature phase transition in the system with $\langle q_i \rangle = 0$, as q_x is varied. Namely, the system becomes superconducting as q_x is increased beyond the critical value q_x^c , which is given by

$$\begin{aligned} q_x^c &\equiv \frac{1}{2} \left(\tilde{C}_{00}^{-1} - \frac{E_J}{2E_0} \right) + \frac{1}{256} \left(\frac{E_J}{E_0} \right)^2 \left(\frac{4N}{\tilde{C}_{00}^{-1} - \tilde{C}_{10}^{-1}} + \sum_{(i,j), j \neq 0} \frac{1}{\tilde{C}_{j0}^{-1} - \tilde{C}_{i0}^{-1} - \tilde{C}_{00}^{-1} + \tilde{C}_{10}^{-1}} \right) \\ &+ \frac{1}{64} \left(\frac{E_J}{E_0} \right)^2 \left(\frac{2}{\tilde{C}_{10}^{-1} - \tilde{C}_{\hat{x}+\hat{y},0}^{-1} - \tilde{C}_{00}^{-1} + \tilde{C}_{10}^{-1}} + \frac{1}{\tilde{C}_{10}^{-1} - \tilde{C}_{2\hat{x},0}^{-1} - \tilde{C}_{00}^{-1} + \tilde{C}_{10}^{-1}} \right). \end{aligned} \quad (17)$$

The resulting phase boundary between the insulating phase and the superconducting phase is shown in Fig. 3, obtained for a 24×24 array. The junction capacitance here tends to enhance superconductivity, which is in accord with the result in Ref. [4]. It is also obvious that as the system approaches the NN charging limit, the insulating region shrinks to zero; *this apparently cures the well-known artifact of the coarse-graining approximation*, where the system remains in the insulating phase for arbitrarily large values of E_J in the NN charging limit [6].

To check the validity of the second-order perturbation expansion, we have computed the third-order contribution in the self-charging limit, and obtain the critical value q_x^c :

$$q_x^c(C_1 = 0) = \frac{1}{2} - \frac{1}{4} \left(\frac{E_J}{E_0} \right) - \frac{3}{128} \left(\frac{E_J}{E_0} \right)^2 - \frac{11}{1024} \left(\frac{E_J}{E_0} \right)^3. \quad (18)$$

The three curves in Fig. 4 represent the phase boundaries obtained from Eq. (18) up to the first-, the second-, and the third-order contributions, respectively. It is shown that the third-order contribution does not change significantly the boundary obtained from the second-order calculation, inducing 8.3% of the difference in the critical value of E_J/E_0 at $q_x = 0$.

We next consider the NN charging limit in the absence of charge frustration ($q_x = 0$). In this case, Eq. (10) gives the energy of the commensurate state in the form

$$E_{(c)} \approx -\frac{E_J^2 N}{8E_1 (\bar{C}_{00}^{-1} - \bar{C}_{10}^{-1})}, \quad (19)$$

where $E_1 \equiv e^2/2C_1$ and

$$\bar{C}_{ij}^{-1} \equiv \frac{1}{N} \sum_{\mathbf{k}} \frac{e^{i\mathbf{k} \cdot (\mathbf{x}_i - \mathbf{x}_j)}}{4 - 2(\cos k_x + \cos k_y)}. \quad (20)$$

In the thermodynamic limit, we replace the discrete sum by the integral and obtain

$$\begin{aligned} \bar{C}_{00}^{-1} - \bar{C}_{10}^{-1} &= \frac{1}{(2\pi)^2} \int_{-\pi}^{\pi} dk_x \int_{-\pi}^{\pi} dk_y \frac{1 - \cos k_x}{4 - 2(\cos k_x + \cos k_y)} \\ &= \frac{1}{2\pi} \int_0^{\pi} dk_x \sqrt{\frac{1 - \cos k_x}{3 - \cos k_x}} = \frac{1}{4}, \end{aligned} \quad (21)$$

leading to $E_{(c)} \approx -E_J^2 N/2E_1$. The first-excited incommensurate state in the NN charging limit is of the CD type (see Fig. 2) with the zeroth-order energy $E_{(ic)}^{(0)} = 8E_1(\bar{C}_{00}^{-1} - \bar{C}_{10}^{-1}) = 2E_1$ and the null first-order energy $E_{(ic)}^{(1)} = 0$. It is complicated but straightforward to calculate $E_{(ic)}^{(2)}$ from the second-order degenerate perturbation theory, which leads to a $4N \times 4N$ matrix. The Fourier transform then yields $N \times 4 \times 4$ Hermitian matrices, each of which can be diagonalized. The lowest eigenvalue then gives the energy of the CD type incommensurate state, up to the second order:

$$E_{(ic)} \approx 2E_1 - \frac{E_J^2}{8E_1} (4N + 62.000), \quad (22)$$

where the number 62.000 has been obtained numerically for a sufficiently large array (1024×1024); at this size finite-size effects have been confirmed to be negligible. The critical value of E_J/E_1 , below which the array is in the insulating phase, is obtained from the condition $E_{(ic)} - E_{(c)} = 0$:

$$\left(\frac{E_J}{E_1} \right)_c \approx 0.508. \quad (23)$$

Note that this value is somewhat larger than the critical value $(E_J/E_1)_c \approx 0.23$ obtained in Refs. [4,11]. One possible explanation of the above discrepancy is the failure of the second-order perturbation expansion. Namely, consideration of higher-order terms may eliminate the discrepancy. The other possibility is that the CD type excitation does not give the true transition point: See Fig. 1 (b) for a schematic picture, where K_1 may correspond to the obtained transition point $(E_J/E_1)_c \approx 0.508$ and K_2 the true transition point. In experiment, the even larger critical value $(E_J/E_1)_c \approx 0.6$ has been obtained [14], via the curve-fit to the square-root cusp form

of the resistance [16]. Recent quantum Monte Carlo simulations, on the other hand, have yielded the result $(E_J/E_1)_c = 0.36 \pm 0.04$.

B. Phase transitions for $\langle q_i \rangle \neq 0$

In the NN charging limit, there exists an interesting duality between the charge and the vortex [11], which concludes that in the absence of the Josephson term, the charges form a superlattice determined by the value of charge frustration q_x . This is a counterpart of the vortex superlattice in the classical array without the charging energy, formed in the presence of magnetic frustration [1,17]. In the system considered here, on the other hand, the non-vanishing self-capacitance gives the interaction range between charges $\Lambda = \sqrt{C_1/C_0}$ in units of the lattice constant, thus making it finite [11]. Accordingly, we expect that the formation of the $q \times q$ charge superlattice with $q \gg \Lambda$ is improbable in the system with the rational charge frustration $q_x = p/q$. This implies that $\langle q_i \rangle$ is not necessarily equal to q_x in the array with non-vanishing C_0 , which reflects that a short-ranged potential in general makes the commensurate phase extend over a finite range of the chemical potential. (Note that the charge frustration in this work plays the role of the chemical potential.)

We now investigate the phase transitions for $\langle q_i \rangle = p/q$ ($\neq 0$), using the canonical ensemble with the total number of charges fixed. To find the zero-temperature phase diagrams we need to know the configurations of the commensurate states and of the lowest-lying incommensurate states, which is a highly nontrivial problem in the 2D system considered here, especially for large q . For the 1D Josephson junction array with $\langle q_i \rangle = 1/q$, the commensurate state, the first excited state, and the resulting zero-temperature phase boundaries have been obtained

via the perturbation expansion [18]. We write the energy of the commensurate state with $\langle q_i \rangle = p/q \neq 0$ in the form

$$E_{(c)}(p/q) = E_{(c)}^{(0)}(p/q) + E_{(c)}^{(1)}(p/q) + E_{(c)}^{(2)}(p/q) + O(E_J^3), \quad (24)$$

where the relations $\sum_i q_i = N\langle q_i \rangle = Np/q$ and $\sum_j \tilde{C}_{ij}^{-1} = 1$ give $E_{(c)}^{(0)}(p/q) = 4E_0 \sum_i q_i \tilde{C}_{ij}^{-1} q_j - 8E_0 q_x N p/q + 4E_0 q_x^2 N$. In general, when $\langle q_i \rangle \neq 0$, the commensurate ground states are degenerate, which makes it necessary to consider the matrix element:

$$V_{lm} \equiv \langle \mathbf{q}^{(l)} | V | \mathbf{q}^{(m)} \rangle = -\frac{E_J}{2} \sum_{\langle i,j \rangle} \left[\prod_{k \neq i,j} \delta(q_k^{(l)}, q_k^{(m)}) \right] \left[\delta(q_i^{(l)}, q_i^{(m)} - 1) \delta(q_j^{(l)}, q_j^{(m)} + 1) + \delta(q_i^{(l)}, q_i^{(m)} + 1) \delta(q_j^{(l)}, q_j^{(m)} - 1) \right] \quad (25)$$

with $|\mathbf{q}^{(l)}\rangle$ being the l th degenerate commensurate state. Note that the configuration of the superlattice unit cell in a degenerate commensurate state is in general different from that in a different (degenerate) state. Therefore, for $l \neq m$, $\mathbf{q}^{(l)}$ differs from $\mathbf{q}^{(m)}$ at the total of $O(N)$ sites for finite q , leading to $V_{lm} = 0$. Further, it is obvious that $V_{ll} = 0$. It is thus concluded that all the components of the matrix V vanish, which results in $E_{(c)}^{(1)}(p/q) = 0$. The second-order contribution is given by

$$E_{(c)}^{(2)}(p/q) = \sum'_{\{\mathbf{q}'\}} \frac{|\langle \mathbf{q}' | V | \mathbf{q} \rangle|^2}{E^{(0)}(\mathbf{q}) - E^{(0)}(\mathbf{q}')}, \quad (26)$$

where $E^{(0)}(\mathbf{q})$ and $E^{(0)}(\mathbf{q}')$ is the zeroth-order energy for given charge configuration \mathbf{q} and \mathbf{q}' , respectively, and the summation \sum' is over the states \mathbf{q}' making the denominator nonzero. The superscript l on \mathbf{q} has been dropped since all the degenerate commensurate states give the same contribution to $E_{(c)}^{(2)}(p/q)$. Namely, the degeneracy is not removed in a finite order since $\mathbf{q}^{(l)}$ and $\mathbf{q}^{(m)}$ cannot be connected by a finite number of charge hoppings. With Eq. (25), Eq. (26) reads

$$E_{(c)}^{(2)}(p/q) = \sum'_{(i,j)} \frac{E_J^2/4}{E^{(0)}(\mathbf{q}) - E^{(0)}(\mathbf{q}_{(i,j)})}, \quad (27)$$

where $\mathbf{q}_{(i,j)} \equiv (q_1, q_2, \dots, q_{i-1}, q_i+1, q_{i+1}, \dots, q_{j-1}, q_j-1, q_{j+1}, \dots, q_N)$ is obtained from \mathbf{q} by a charge hopping between sites i and j . It is easy to compute the denominator in Eq. (27):

$$\begin{aligned} E^{(0)}(\mathbf{q}) - E^{(0)}(\mathbf{q}_{(i,j)}) &= 4E_0 \sum_{k,l} \left[(q_k - q_x) \tilde{C}_{kl}^{-1} (q_l - q_x) - (q_{(i,j),k} - q_x) \tilde{C}_{kl}^{-1} (q_{(i,j),l} - q_x) \right] \\ &= 8E_0 \left[\sum_l \left(\tilde{C}_{jl}^{-1} - \tilde{C}_{il}^{-1} \right) q_l - \left(\tilde{C}_{00}^{-1} - \tilde{C}_{10}^{-1} \right) \right], \end{aligned} \quad (28)$$

which leads to the expression for the energy of the commensurate state with $\langle q_i \rangle = p/q$:

$$\begin{aligned} E_{(c)}(p/q) &\approx 4E_0 \sum_{i,j} q_i \tilde{C}_{ij}^{-1} q_j - 8E_0 q_x N \frac{p}{q} + 4E_0 q_x^2 N \\ &+ \frac{E_J^2}{32E_0} \sum'_{(i,j)} \frac{1}{\sum_l \left(\tilde{C}_{jl}^{-1} - \tilde{C}_{il}^{-1} \right) q_l - \left(\tilde{C}_{00}^{-1} - \tilde{C}_{10}^{-1} \right)}. \end{aligned} \quad (29)$$

Here q_i is the charge at site i in the commensurate state with $\langle q_i \rangle = p/q$. Since the (commensurate) ground state configurations are not known for general p/q , q_i in this work is obtained via the simulated annealing method.

To compute the energies of the incommensurate states with $\langle q_i \rangle = p/q \neq 0$, we classify excitations according to the number q_e of extra charges (with the sign taken into account), and let $E_{(ic)}(p/q, q_e)$ denote the energy of this excited state which has the total number of charges $Np/q + q_e$. To the second order in E_J , it is straightforward to obtain the energy of the q_e -charge excited state:

$$\begin{aligned}
E_{(ic)}(p/q, q_e) \approx & 4E_0 \sum_{i,j} q_i^{(q_e)} \tilde{C}_{ij}^{-1} q_j^{(q_e)} - 8E_0 q_x \left(N \frac{p}{q} + q_e \right) + 4E_0 q_x^2 N \\
& + \frac{E_J^2}{32E_0} \sum'_{(i,j)} \frac{1}{\sum_l (\tilde{C}_{jl}^{-1} - \tilde{C}_{il}^{-1}) q_l^{(q_e)} - (\tilde{C}_{00}^{-1} - \tilde{C}_{10}^{-1})},
\end{aligned} \tag{30}$$

where $q_i^{(q_e)}$ is the charge at site i in the q_e -charge excited state, and the first-order contribution $E_{(ic)}^{(1)}(p/q, q_e)$ has been observed to vanish in numerical calculations, regardless of the values of p/q ($\neq 0$) and q_e considered in this work. Further, in Eq. (30), we have assumed that degeneracy is not removed in the second order although there are some exceptions, e.g., for $p/q=1/2$ and $q_e = -1$ (see below). To find the phase boundary, we need to know the charge configuration which corresponds to the first excited state for given values of C_1/C_0 and q_x . For this purpose, we use the following numerical procedure:

1. Distribute $Np/q + q_e$ charges randomly.
2. Use the simulated annealing method to find the charge configuration $q_i^{(q_e)}$, which minimizes the zeroth-order energy $4E_0 \sum_{i,j} q_i^{(q_e)} \tilde{C}_{ij}^{-1} q_j^{(q_e)} - 8E_0 q_x (Np/q + q_e)$.
3. Change the value of q_e , and repeat the steps 1 - 3.
4. Among the obtained charge configurations with their zeroth-order energies, find one corresponding to the lowest-lying incommensurate state.

In the numerical simulations, we have used the conventional simulated annealing method adopting the Metropolis algorithm for the arrays of sizes 10×10 and 12×12 . Starting from high temperatures ($T > 1.0$), we decrease the temperature slowly with the decrements $\Delta T = 0.1$ (at high temperatures) and 0.002 (at low temperatures), and perform 10000 MC steps per site at each temperature step. We have found that the charge configuration corresponding to the lowest energy depends crucially on the value of C_1/C_0 , and thus used three different values: $C_1/C_0 = 0.1, 1.0, \text{ and } 5.0$. Through 20 independent runs, we have obtained the charge configurations corresponding to the lowest energy, which have also been checked via the entropic annealing algorithm [19]. Although we have allowed double occupancy ($q_i = 2$) as well, in the lowest-lying configurations q_i is always found to have the value either 0 or 1.

Once the charge configuration $q_i^{(q_e)}$ which minimizes the zeroth-order energy in Eq. (30) is found, the phase boundary is determined from the condition $E_{(c)}(p/q) = E_{(ic)}(p/q, q_e)$. This leads to the critical value q_x^c separating the superconducting phase from the insulating phase:

$$\begin{aligned}
q_x^c \equiv & \frac{1}{2q_e} \left[\sum_{i,j} \tilde{C}_{ij}^{-1} (q_i^{(q_e)} q_j^{(q_e)} - q_i q_j) \right] \\
& + \frac{(E_J/E_0)^2}{256q_e} \left[\sum'_{(i,j)} \frac{1}{\sum_l (\tilde{C}_{jl}^{-1} - \tilde{C}_{il}^{-1}) q_l^{(q_e)} - (\tilde{C}_{00}^{-1} - \tilde{C}_{10}^{-1})} \right. \\
& \left. - \sum'_{(i,j)} \frac{1}{\sum_l (\tilde{C}_{jl}^{-1} - \tilde{C}_{il}^{-1}) q_l - (\tilde{C}_{00}^{-1} - \tilde{C}_{10}^{-1})} \right],
\end{aligned} \tag{31}$$

where $\{q_i\}$ again describes the charge configuration of the commensurate state. When $q_e < 0$, the system, displaying superconductivity for $q_x < q_x^c$, becomes insulating as q_x is increased beyond q_x^c . This behavior according to whether q_x is larger or smaller than q_x^c is reversed when $q_e > 0$.

Table I shows the values of q_e in the lowest excitations, breaking the commensurability of the states with $\langle q_i \rangle = 1/2, 1/3, 1/4, \text{ and } 1/5$, in the arrays of sizes $L = 10$ and 12 . Except for $\langle q_i \rangle = 1/2$, there are two values of q_e in

each case, one for the positive-charge excitation ($q_e > 0$) and the other for the negative-charge excitation ($q_e < 0$). Since the value of the charge frustration has been restricted in the range $0 \leq q_x < 1/2$, we need to consider only the negative-charge excitations for $\langle q_i \rangle = 1/2$. It displays that as C_1 is increased, the absolute value of q_e decreases, manifesting that the excitations become more point-like. As an example, we present the charge configurations for $\langle q_i \rangle = 1/2$ in Fig. 5, where (a), (b), and (c) correspond to the commensurate state, the excited state

with $q_e = -1$, and the excited state with $q_e = -12$, respectively, in a 12×12 array. It is of interest to note that the configuration (c), which has 60 charges, is precisely the same as the ground state configuration of vortices in the presence of the magnetic frustration $5/12$ [17]. When $q_e = -1$ is the lowest excitation, there exists $N/2$ -fold degeneracy since the vacant site, represented by a small

square in (b), can be located on any of the total $N/2$ sites. In this case, the degenerate states are coupled in $O(E_J^2)$, and we should use the second-order degenerate perturbation theory to calculate the energy. It is again straightforward to diagonalize the second-order matrix by means of the Fourier transform, which yields

$$\begin{aligned}
E_{(ic)}(1/2, -1) \approx & 4E_0 \sum_{i,j} q_i^{(-1)} \tilde{C}_{ij}^{-1} q_j^{(-1)} - 8E_0 q_x \left(\frac{1}{2}N - 1 \right) + 4E_0 q_x^2 N \\
& + \frac{E_J^2}{32E_0} \left[\sum'_{(i,j)} \frac{1}{\sum_l (\tilde{C}_{jl}^{-1} - \tilde{C}_{il}^{-1}) q_l^{(-1)} - \tilde{C}_{00}^{-1} + \tilde{C}_{10}^{-1}} \right. \\
& + \frac{12}{\sum_l (\tilde{C}_{k+\hat{x},l}^{-1} - \tilde{C}_{kl}^{-1}) q_l^{(-1)} - \tilde{C}_{00}^{-1} + \tilde{C}_{10}^{-1}} \\
& + \frac{8}{\sum_l (\tilde{C}_{k+\hat{x}+\hat{y},l}^{-1} - \tilde{C}_{k+\hat{x},l}^{-1}) q_l^{(-1)} - \tilde{C}_{00}^{-1} + \tilde{C}_{10}^{-1}} \\
& \left. + \frac{4}{\sum_l (\tilde{C}_{k+2\hat{x},l}^{-1} - \tilde{C}_{k+\hat{x},l}^{-1}) q_l^{(-1)} - \tilde{C}_{00}^{-1} + \tilde{C}_{10}^{-1}} \right], \tag{32}
\end{aligned}$$

in place of Eq. (30). Here k denotes the position of the vacant site.

Figure 6 shows the resulting phase diagrams for $C_1/C_0 =$ (a) 0.1, (b) 1.0, and (c) 5.0. The various lobe-like structures, in which the array is in insulating phase, are obtained. Since the screening length $\Lambda = \sqrt{C_1/C_0}$, beyond which the magnitude of the interaction between charges decreases exponentially, is much smaller than the system size, the finite-size effects on the phase boundaries are presumably negligible. We have checked the phase boundary for $\langle q_i \rangle = 1/2$, and indeed found that it hardly changes with the system size considered here (see below). Accordingly, the phase boundaries in Fig. 6 are expected to be qualitatively correct even in the thermodynamic limit. As we increase the array size, more insulating lobes should be observed, since the array with $E_J = 0$ should be insulating, regardless of the value of q_x . At this stage, however, it is still unclear whether the insulating lobe exists at every rational value of q_x . In the NN charging limit, the charging-energy term takes the form $H_0 = 4E_1 \sum_{i,j} (q_i - q_x) \tilde{C}_{ij}^{-1} (q_j - q_x)$ with \tilde{C}_{ij}^{-1} given by Eq. (20). Here the divergence of \tilde{C}_{00}^{-1} leads to $\langle q_i \rangle = q_x$, which is simply the counterpart of the vortex-neutrality condition in the classical array. Indeed Fig. 6 shows that the position of the insulating region approaches $\langle q_i \rangle = q_x$, as C_1/C_0 is increased.

To study the effects of the junction capacitance versus the self-capacitance in detail, we now concentrate on the $\langle q_i \rangle = 1/2$ insulating phase, whose commensurate charge

configuration displays the 2×2 superlattice structure. [See Fig. 5 (a).] Similarly to the vortex superlattice in the fully-frustrated classical array [20], the commensurate state has the two-fold degeneracy. If we remove a single positive charge from the system, commensurability is destroyed near the resulting point defect. The charge configuration of the corresponding lowest-lying incommensurate state has been shown in Fig. 5 (b), which describes the first excited state for $C_1/C_0 = 1.0$ or 5.0 . When $C_1/C_0 = 0.1$, in contrast, the first excited state has the configuration shown in Fig. 5 (c), with the number of extra charge $q_e = -12$. This observation that the nature of the lowest excited state changes with C_1/C_0 has an important implication with regard to the supersolid phase, where a commensurate charge-density wave is believed to coexist with superfluidity [9,10]: The charge configuration in Fig. 5 (b) regarded as a snapshot of the charge configuration in the supersolid phase demonstrates that the underlying global commensurability still holds despite of the local point defect. Furthermore, since the point defect can hop to any site without energy cost, it is delocalized in the energy eigenstate, leading to superfluidity. Accordingly, we conclude that the existence of the supersolid phase depends on the value of C_1/C_0 . In particular, when C_1/C_0 is sufficiently small, the supersolid phase does not exist. It is of interest to compare this argument pointing out the importance of the vacant defect in supersolidity with that of Ref. [10], emphasizing the role of the double occupancy. In the numerical inves-

tigations to find the lowest-energy charge configurations, we have found that all the charges have the value either 0 or 1 at zero temperature, and that those configurations with $q_i = -1$ or 2 at some sites have much higher energies. The $\langle q_i \rangle = 1/2$ phase boundaries in Fig. 6 (b) and (c) may be considered to divide the insulating commensurate phase and the supersolid phase. As we go further into the supersolid phase starting from the phase boundary, the more point defects are generated; the commensurability should be completely destroyed when we cross another phase boundary separating the supersolid phase from the superfluid phase, although within the formalism adopted here, we are unable to find this new boundary. To obtain the phase diagram for $\langle q_i \rangle = 1/2$, we have considered $L \times L$ arrays up to $L = 24$, and found that the finite-size effects are negligible for $C_1/C_0 \lesssim 10$, which corresponds to the interaction range $\Lambda \lesssim \sqrt{10} \ll L$, and that the qualitative features of the phase diagram do not change even when $C_1/C_0 \gtrsim 10$.

We have further found that the difference between the phase boundary obtained from the excitation $q_e = -1$ and that from $q_e = -12$ is insignificant in the 12×12 array with $C_1/C_0 = 0.1$. Therefore, for simplicity, we consider only the excitation $q_e = -1$ and compute the phase boundary from Eqs. (29) and (32). The resulting phase diagram obtained for the array of size $L = 24$ is shown in Fig. 7. The insulating region is shown to expand with C_1/C_0 when $C_1/C_0 \lesssim 0.1$ and then to shrink as C_1/C_0 is increased further. This is to be compared with the case $\langle q_i \rangle = 0$ (shown in Fig. 3), where superconductivity is enhanced monotonically with C_1/C_0 , even for small C_1/C_0 .

IV. FINITE-TEMPERATURE PHASE DIAGRAMS

In this section, we investigate the phase transitions of the superconducting arrays at finite temperatures, where thermal fluctuations as well as quantum fluctuations suppress the ordering of phases. While at high temperatures the system should be in the normal (disordered) state due to large thermal fluctuations, strong charging effects at low temperatures produce large quantum fluctuations, tending to destroy superconductivity of the system. We thus expect rich behaviors resulting from the interplay of thermal and quantum fluctuations, which may be controlled by the temperature and charging energy. We first study the system in the absence of the Josephson coupling via MC simulations, and then investigate the phase transitions in the presence of the Josephson coupling via a variational method together with MC simulations.

A. Superconducting array without Josephson coupling

In the absence of the Josephson coupling ($E_J = 0$), the Hamiltonian is diagonal in the charge representation and written in the form

$$H = 4E_0 \sum_{i,j} q_i \tilde{C}_{ij}^{-1} q_j - 8E_0 q_x \sum_i q_i, \quad (33)$$

where q_i is the eigenvalue of the charge operator at site i . We perform MC simulations on the above Hamiltonian to investigate how the insulating phase corresponding to the regions inside the lobes in Fig. 6 changes with the temperature. Using the conventional MC method with the Metropolis algorithm, we start from a sufficiently high temperature ($T = 1.0$), and decrease the temperature slowly with the decrements $\Delta T = 0.1$ (at high temperatures) and 0.002 (at low temperatures). During the simulations, we allow creation and annihilation of a charge at a site, as well as hopping to other sites. At each temperature step, we compute the thermal average $\langle q_i \rangle_T$ using 10000 MC steps per site, after 1000 MC steps of equilibration.

Figure 8 displays the results for arrays of sizes $L = 10$ (left) and 12 (right), with $C_1/C_0 =$ (a) 0.1, (b) 1.0, and (c) 5.0. At zero temperature, the curves representing $\langle q_i \rangle$ versus q_x exhibit steps at rational values giving the (commensurate) insulating phase. Such step structures, which correspond to the lobe structures in Fig. 6, are common in systems displaying commensurate-incommensurate transitions, and signal the commensurate locking [21]. It is shown that, as expected, the width of a step decreases with C_1/C_0 , and the curve approaches the straight line $\langle q_i \rangle = q_x$ in the limit $C_1/C_0 \rightarrow \infty$, manifesting the suppression of the insulating phase. Comparing the results for the $L = 10$ array with those for the $L = 12$ array, we also expect more rational steps in larger arrays, which is apparently suggestive of the devil's staircase structure [21] in the thermodynamic limit. For conclusive results, however, more detailed study is needed. Table II presents the widths of the rational steps of $\langle q_i \rangle = 0, 1/3$, and $1/2$ in the $L = 12$ array at zero temperature. One can see here that the values in Table II are in good agreement with the $E_J = 0$ results in Fig. 6, which supports the validity of the approach in Sec. III.

Figure 8 also shows that steps tend to disappear at finite temperatures, reflecting that thermal fluctuations suppress the charge ordering due to quantum coherence as well as the phase ordering. Accordingly, the insulating commensurate phase in general turns into the normal (disordered) phase as the temperature is increased from zero. Note, however, that some steps survive weak thermal fluctuations. Namely, whereas steps at higher-order rationals easily disappear, low-order steps such as $\langle q_i \rangle = 0, 2$, and $1/3$ persist at low but nonzero temperatures. These features presumably can also be observed in the systems with nonzero Josephson couplings. Thus

as we increase the temperature from zero, higher-order insulating lobes in Fig. 6 disappear, but some low-order lobes are expected to remain at low temperatures.

B. Superconducting array with Josephson coupling

In the presence of the Josephson coupling, both the charge and the phase variables should be treated quantum-mechanically, which prohibits exact analytical treatment. Here, we use the Giachetti-Tognetti-Feynman-Kleinert (GTFK) variational method [22] to evaluate the path integral and to obtain the effective classical Hamiltonian, which is convenient for studying the phase transitions at finite temperatures. The GTFK method, which remains reliable in known cases even at zero temperature, has been successfully applied to the superconducting arrays with continuous charge states in

the presence of Ohmic dissipation [4,23]. We begin with the Hamiltonian given by Eq. (3) and write the partition function of the system in terms of the path integral [24]:

$$Z = \prod_i \int d\phi_i(0) \int \mathcal{D}\phi_i(\tau) \exp \{-S_E[\phi_i(\tau)]\} \quad (34)$$

with the Euclidean action

$$S_E = \int_0^\beta d\tau L_E(\tau), \quad (35)$$

where $\beta \equiv 1/k_B T$ is the inverse temperature, and the Planck constant has been set equal to unity ($\hbar \equiv 1$). The Euclidean Lagrangian L_E can be obtained from the Hamiltonian via the Wick rotation $t \rightarrow -i\tau$ and the Legendre transformation. We use the representation $q_i = -i\partial/\partial\phi_i$ obeying the commutation relation $[\phi_i, q_i] = i$, and get

$$L_E = \frac{1}{16E_0} \sum_{i,j} \dot{\phi}_i \tilde{C}_{ij} \dot{\phi}_j - iq_x \sum_i \dot{\phi}_i - E_J \sum_{\langle i,j \rangle} \cos(\phi_i - \phi_j) \quad (36)$$

with $\dot{\phi}_i \equiv \partial\phi_i/\partial\tau$, where the charge frustration enters through a purely imaginary term.

In the presence of Ohmic dissipation, the charge at each site takes continuous values, and only the paths satisfying $\phi_i(\beta) = \phi_i(0)$ contribute to the partition function, with the dissipative action term added [4,25]. In this case, the charge frustration does not appear in the Euclidean action since $\int_0^\beta d\tau \dot{\phi}_i = 0$, and the resulting phase diagram does not depend on q_x . If there is no Ohmic dissipation present, in contrast, only discrete charge states are allowed, and all the paths satisfying $\phi_i(\beta) = \phi_i(0) + 2\pi n_i$ with integer n_i contribute to the path integral in Eq. (34) [25]. Therefore the path integral should include the summation over the ‘‘winding numbers’’ $\{n_i\}$, yielding interesting behaviors associated with the charge frustration [6]. Accordingly, the allowed charge states, i.e., continuous or discrete, are crucial in the resulting phase diagrams.

From the boundary condition $\phi_i(\beta) = \phi_i(0) + 2\pi n_i$, we decompose ϕ_i into the periodic variable θ_i satisfying $\theta_i(\beta) = \theta_i(0)$ and n_i , according to $\phi_i(\tau) \equiv \theta_i(\tau) + (2\pi\tau/\beta)n_i$, and obtain the Euclidean action in the form

$$S_E = \frac{\pi^2}{4\beta E_0} \sum_{i,j} n_i \tilde{C}_{ij} n_j - i2\pi q_x \sum_i n_i + S_{ph}, \quad (37)$$

where

$$S_{ph} \equiv \int_0^\beta d\tau \left\{ \frac{1}{16E_0} \sum_{i,j} \dot{\theta}_i \tilde{C}_{ij} \dot{\theta}_j - E_J \sum_{\langle i,j \rangle} \cos \left[\theta_i - \theta_j + \frac{2\pi\tau}{\beta} (n_i - n_j) \right] \right\}.$$

Following the GTFK method, it is straightforward to obtain the effective classical Hamiltonian

$$-\beta H_{cl} = -\frac{\pi^2}{4\beta E_0} \sum_{i,j} n_i \tilde{C}_{ij} n_j + i2\pi q_x \sum_i n_i + g\beta E_J \sum_{\langle i,j \rangle} \cos(\theta_i - \theta_j) \delta_{n_i, n_j}, \quad (38)$$

where g is determined by

$$g = g_0 (1 - \log g_0) \\ -\log g_0 = \frac{\beta E_0}{\pi^2} \sum_{n=1}^{\infty} \left\{ \left[\left(1 + \frac{2C_1}{C_0} \right) n^2 + \frac{4g_0\beta^2 E_J E_0}{\pi^2} \right]^{-1} \right.$$

$$\begin{aligned}
& + \left\{ \left(\frac{1}{3} + \frac{2C_1}{C_0} \right) n^2 + \frac{4g_0\beta^2 E_J E_0}{\pi^2} \right\}^{-1} \\
& = \frac{1}{8g_0\beta E_J} (x_1 \coth x_1 + x_2 \coth x_2 - 2)
\end{aligned} \tag{39}$$

with $x_1 \equiv \sqrt{4g_0\beta^2 E_J E_0 / (1 + 2C_1/C_0)}$ and $x_2 \equiv \sqrt{4g_0\beta^2 E_J E_0 / (1/3 + 2C_1/C_0)}$. Here we have used identity

$$\sum_{n=1}^{\infty} \frac{1}{n^2 + (x/\pi)^2} = \frac{\pi^2}{2x^2} (x \coth x - 1).$$

When Eq. (39) has more than one zeros, we should choose the largest one according to the extremal principle. The detailed procedure is entirely similar to that in Ref. [4], and will not be repeated here. As a result, the quantum fluctuations renormalize the Josephson coupling E_J to gE_J . Furthermore, in contrast to the continuous charge case [4], the charge frustration appears explicitly in the Hamiltonian, and is expected to play an important role in the phase transition of the system.

Unfortunately, the Kronecker delta δ_{n_i, n_j} between winding numbers of nearest neighboring pairs in Eq. (38) makes further analysis very difficult. For simplicity, we thus replace it by its self-consistent average δ and obtain the approximate Hamiltonian

$$-\beta H'_{cl} = -\frac{\pi^2}{4\beta E_0} \sum_{i,j} n_i \tilde{C}_{ij} n_j + i2\pi q_x \sum_i n_i + g\delta\beta E_J \sum_{\langle i,j \rangle} \cos(\theta_i - \theta_j), \tag{40}$$

where

$$\delta \equiv \langle \delta_{n_i, n_j} \rangle \equiv \frac{\text{Tr} \delta_{n_i, n_j} e^{-\beta H'_{cl}}}{\text{Tr} e^{-\beta H'_{cl}}}$$

is the ensemble average with respect to the approximate Hamiltonian H'_{cl} . The Poisson summation formula then allows us to write

$$\delta = \frac{\int_0^1 dx \sum_{\{m_i\}} \exp \left[-4\beta E_0 \sum_{i,j} (m_i - q_x - q'_i(x)) \tilde{C}_{ij}^{-1} (m_j - q_x - q'_j(x)) \right]}{\sum_{\{m_i\}} \exp \left[-4\beta E_0 \sum_{i,j} (m_i - q_x) \tilde{C}_{ij}^{-1} (m_j - q_x) \right]} \tag{41}$$

with $q'_i(x) \equiv x(\delta_{i,1} - \delta_{i,2})$, which manifests the absence of dependence on E_J . Once δ is determined from Eq. (41), the partition function of the system obtains the form

$$Z = Z_{ch} Z_{ph}, \tag{42}$$

where the charge-part

$$Z_{ch} = \sum_{\{q_i\}} \exp \left[-4\beta E_0 \sum_{i,j} (q_i - q_x) \tilde{C}_{ij}^{-1} (q_j - q_x) \right]$$

has been obtained from the Poisson summation formula and the phase-part is given by

$$Z_{ph} = \int \prod_i d\theta_i \exp \left[-g\delta\beta E_J \sum_{\langle i,j \rangle} \cos(\theta_i - \theta_j) \right].$$

Unless the ratio C_1/C_0 is infinite, the interaction \tilde{C}_{ij}^{-1} between charges is short-ranged and does not have any

singularity. It is then reasonable to assume that the criticality of the system is governed by the phase-part, which implies that the system exhibits a vortex-unbinding BKT transition at the critical temperature given by [26]

$$g\delta\beta E_J \approx 1/0.9. \tag{43}$$

We first consider the self-charging limit ($C_1 = 0$). In this limit, δ can easily be evaluated since the terms in Eq. (41) factorize. The resulting phase diagrams determined from Eq. (43) at temperatures $T = 0.1, 0.2, 0.5, 0.7$, and 1.0 (in units of E_0/k_B) are shown in Fig. 9. The region in the right-hand side of each line corresponds to the superconducting phase whereas the left region represents the normal (disordered) phase. In this phase diagram, we observe that the superconducting region expands as q_x is increased at all temperatures. (Recall that the symmetry of the system allows to restrict within the range $[0, 1/2]$.) Therefore it is concluded that the charge frustration in general enhances superconductivity. The qualitative features are largely similar to

those of the results from the coarse-graining approach [6] at temperatures $T > 0.2$. Unlike the latter, however, Fig. 9 also shows reentrant behavior at low temperatures, for small q_x . At zero temperature, unfortunately, we obtain the unphysical result that the system is in the superconducting state for $1/3 \leq q_x \leq 2/3$, even in the limit of the vanishing Josephson coupling. This is presumably an artifact of the self-consistent approximation (SCA) replacing of the Kronecker delta by its average, with correlations neglected.

When $C_1/C_0 \neq 0$, on the other hand, the terms in Eq. (41) do not factorize, and the average δ cannot be evaluated analytically, which makes it inevitable to resort to a numerical method. At extremely low temperatures, m_i in Eq. (41) can have the value either 0 or 1, which allows us to calculate δ by direct summation of 2^N terms for small L . At high temperatures, other values of m_i are allowed; this makes the direct summation im-

practical and we use MC simulations. Figure 10 shows the resulting phase diagram obtained for a 4×4 array with $C_1/C_0 = 1.0$ at temperature $T = 0.1, 0.2, 0.3,$ and 0.4 . At $T = 0.1$, δ has been calculated by means of both the direct summation with $m_i = 0$ and 1 and MC simulations, which give results in good agreement with each other. At higher temperatures, δ has been obtained via MC simulations, yielding the enhancement of superconductivity by charge frustration in a similar manner to that in the self-charging limit. At low temperatures ($T = 0.1$), on the other hand, there exists a small lobe near $q_x = 1/2$, which indicates the expansion of the insulating region due to the commensurability effects on the ordering of charges.

To check the validity of the SCA adopted here, replacement of δ_{n_i, n_j} to its self-consistent value δ , we have performed MC simulations with $q_x = 0$, at which the Hamiltonian in Eq. (38) has only real terms:

$$-\beta H_{cl} = -\frac{\pi^2}{4\beta E_0} \sum_{i,j} n_i \tilde{C}_{ij} n_j + g\beta E_J \sum_{\langle i,j \rangle} \cos(\theta_i - \theta_j) \delta_{n_i, n_j}. \quad (44)$$

We have considered a 16×16 array with various values of E_J/E_0 , and measured the helicity modulus Υ with 100000 MC steps:

$$\Upsilon \equiv \frac{1}{N} \left[\left\langle \sum_{\langle i,j \rangle} x_{ij}^2 \cos(\theta_i - \theta_j) \right\rangle - \beta E_J \left\langle \left(\sum_{\langle i,j \rangle} x_{ij} \sin(\theta_i - \theta_j) \right)^2 \right\rangle + \beta E_J \left\langle \sum_{\langle i,j \rangle} x_{ij} \sin(\theta_i - \theta_j) \right\rangle^2 \right], \quad (45)$$

where $x_{ij} \equiv x_j - x_i$ with x_i denoting the x coordinate of the i th grain in units of the lattice constant. The universal jump condition of the helicity modulus [27]

$$\Upsilon = 2/\pi\beta E_J = 2TE_0/\pi E_J \quad (46)$$

then determines the critical coupling $(E_J/E_0)_c$, the values of which are displayed in Table III, for $C_1/C_0 = 0$ and 1 at various temperatures. Table III also displays the results from the SCA replacing the Kronecker delta by its average, which has yielded Figs. 9 and 10: The two results indeed exhibit behaviors qualitatively in accord with each other. In particular, for $C_1/C_0 = 0$, both results give the value of $(E_J/E_0)_c$ larger at $T = 0.1$ than at $T = 0.2$, strongly suggesting the reentrant transition.

From a quantitative viewpoint, on the other hand, the agreement between the two results is not satisfactory, especially at low temperatures, which seems to indicate that the SCA fails at low temperatures. To examine this, we have also measured in the MC simulations the average value of δ_{n_i, n_j} for $C_1 = 0$ and display the results

in Fig. 11. At high temperatures, the MC data indeed agree well with the results from Eq. (41) which is represented by the solid line in Fig. 11. However, at low temperatures the difference is apparent unless E_J/E_0 is sufficiently small. In particular, for $E_J \gtrsim E_0$, the MC simulations give the value approaching unity as the temperature is decreased to zero, whereas the value from Eq. (41) approaches zero. This is the case that the second term in Eq. (44) is dominant over the first term, which leads to the ordering of both $\{\theta_i\}$ and $\{n_i\}$. This reflects strong correlations between the two, which have not been taken into account in the SCA. It is thus concluded that the *quantitative* behaviors of the phase diagrams in Fig. 9 are accurate only at sufficiently high temperatures as already shown in Table III.

V. CONCLUSION

We have investigated the quantum phase transitions in two-dimensional superconducting arrays with various values of external charge frustration at both zero and finite temperatures. We have considered general capacitance matrices, allowing both the self- and the junction capacitances. In the absence of dissipation, the charge variable in the array changes in discrete quanta of $2e$, and the phase variable becomes compact in the interval $[-\pi, \pi)$. We have studied in detail zero-temperature phase transitions at various values of the charge density and also considered the system at finite temperatures with and without the Josephson energy.

The states of the system at zero temperature have been determined from the investigation of the crossing of the ground-state level and the first-excited-state level. At vanishing charge density ($\langle q_i \rangle = 0$), we have considered the commensurate insulating state, where $q_i = 0$ at all sites, and two types of the incommensurate superconducting state, i.e., the single-charge (SC) type and the charge-dipole (CD) type. Unless the self-capacitance vanishes, the SC type incommensurate state has been found to have lower energy than the CD type one except at very small values of the charge frustration. From the comparison of the energies of the commensurate insulating state and the SC type superconducting state, computed via the second-order perturbation expansions, the phase boundary has been obtained. The validity of the second-order expansion has been checked for the array in the self-charging limit, which reveals that the inclusion of the third-order term does not change significantly the phase diagram. At finite charge densities, identification of the commensurate state and of the first-excited incommensurate state is a highly nontrivial problem. We have thus adopted the simulated annealing method and applied the second-order perturbation theory to obtain a number of lobe-like insulating phases such as $\langle q_i \rangle = 1/2, 1/3, 1/4,$ and $1/5$ in 10×10 and 12×12 arrays. As the system size is increased, more insulating lobes are expected to be observed. The effects of the junction capacitance have been investigated in detail in the insulating phases of $\langle q_i \rangle = 0$ and $1/2$: As C_1/C_0 is increased, the insulating region shrinks monotonically for $\langle q_i \rangle = 0$, while the insulating region for $\langle q_i \rangle = 1/2$ expands with C_1 and then shrinks, with its maximum area at $C_1/C_0 \approx 0.1$. The MC simulations have displayed that the lowest excited state changes as the junction capacitance is increased, which in turn indicates that the existence of the supersolid phase with $\langle q_i \rangle = 1/2$ depends on the interaction range of charges: The supersolid phase exists for sufficiently large values of the ratio of the junction capacitance to the self-capacitance. In the supersolid phase, it has also been shown that the point defect in the charge configuration plays an important role.

At finite temperatures, thermal fluctuations as well as quantum fluctuations play an important role in the

phase transitions of the system. In the limit of vanishing Josephson coupling strength, we have performed the MC simulations to obtain $\langle q_i \rangle$ as functions of the charge frustration at various temperatures, and pointed out the possibility of the devil's staircase structure in the thermodynamic limit. As the temperature is increased, higher-order insulating states disappear but some lower-order ones still remain at sufficiently low temperatures. In the presence of the Josephson coupling, we have obtained the effective classical Hamiltonian via a variational method in the path integral formalism. A self-consistent approximation has been applied to the resulting Hamiltonian and phase boundaries have been computed for $C_1/C_0 = 0$ and 1. A reentrant transition at $q_x = 0$ has been observed for the array in the self-charging limit ($C_1 = 0$), while an insulating lobe-like structure has been found near $q_x = 0.5$ in the case $C_1/C_0 = 1.0$. The validity of the formalism used here, the self-consistent approximation (SCA) on the effective classical Hamiltonian, has been checked using MC simulations in the absence of charge frustration. Although the reentrant behavior of the array in the self-charging limit has also been observed in MC simulations, the SCA appears to be accurate only at sufficiently high temperatures.

The quantum phase transitions of the superconducting arrays have been studied theoretically by many authors via mean-field approximations such as the coarse-graining approximation [6] and via the semiclassical methods including the variational methods [4,10] and the WKB approximation [5]. Although the mean-field approximations are in general expected to give better results at zero temperature, where the dimension of the system is effectively increased by one, than at finite temperatures, it is well known that the coarse-graining approximation gives unphysical results even at zero temperature, for the arrays without self-capacitances. On the other hand, the semiclassical methods should be applied with great care at zero temperature, where quantum fluctuations are strong. In comparison with these methods, the formalism adopted here to study the zero-temperature phase transitions, perturbation expansion combined with simulated annealing, appears to be more reliable and can be applied to other systems systematically.

ACKNOWLEDGMENTS

We thank G.S. Jeon for useful discussions. This work was supported in part by the Basic Science Research Institute Program, Ministry of Education, and in part by the Korea Science and Engineering Foundation through the SRC Program.

- [1] For a list of references, see, e.g., *Proceedings of the 2nd CTP workshop on Statistical Physics: KT Transition and Superconducting Arrays*, edited by D. Kim, J.S. Chung, and M.Y. Choi (Min-Eum Sa, Seoul, 1993); *Physica B* **222** 253-406 (1996).
- [2] V.L. Berezinskii, *Zh. Eksp. Teor. Fiz.* **59**, 907 (1970) [*Sov. Phys. JETP* **32**, 493 (1971)]; J.M. Kosterlitz and D.J. Thouless, *J. Phys. C* **6**, 1181 (1973); J.M. Kosterlitz, *J. Phys. C* **7**, 1046 (1974); J.V. José, L.P. Kadanoff, S. Kirkpatrick, and D.R. Nelson, *Phys. Rev. B* **16**, 1217 (1977).
- [3] L.J. Geerligs, M. Peters, L.E.M. de Groot, A. Verbruggen, and J.E. Mooij, *Phys. Rev. Lett.* **63**, 326 (1989); H.S.J. van der Zant, L.J. Geerligs, and J. E. Mooij, *Europhys. Lett.* **19**, 541 (1992).
- [4] B.J. Kim and M.Y. Choi, *Phys. Rev. B* **52**, 3624 (1995).
- [5] C. Rojas and V. José, *Phys. Rev. B* **54**, 12361 (1996).
- [6] C. Bruder, R. Fazio, A. Kampf, A. van Otterlo, and G. Schön, *Phys. Scr. T* **42**, 159 (1992); A. van Otterlo, K.-H. Wagenblast, R. Fazio, and G. Schön, *Phys. Rev. B* **48**, 3316 (1993).
- [7] M.P.A. Fisher, P.B. Weichman, G. Grinstein, and D.S. Fisher, *Phys. Rev. B* **40**, 546 (1989); G.G. Batrouni, R.T. Scalettar, and G.T. Zimanyi, *Phys. Rev. Lett.* **65**, 1765 (1990).
- [8] J.K. Freericks and H. Monien, *Europhys. Lett.* **26**, 545 (1994).
- [9] M.W. Meisel, *Physica B* **178**, 121 (1992); G.G. Batrouni, R.T. Scalettar, G.T. Zimanyi, and A.P. Kampf, *Phys. Rev. Lett.* **74**, 2527 (1995); A. van Otterlo and K.-H. Wagenblast, *ibid.* **72**, 3598 (1994); E. Roddick and D. Stroud, *Phys. Rev. B* **51**, 8672 (1995).
- [10] A. van Otterlo, K.-H. Wagenblast, R. Baltin, C. Bruder, R. Fazio, and G. Schön, *Phys. Rev. B* **52**, 16176 (1995).
- [11] L.V. Keldysh, *Pis'ma Zh. Eksp. Teor. Fiz.* **29**, 716 (1979) [*JETP Lett.* **29**, 658 (1979)]; R. Fazio and G. Schön, *Phys. Rev. B* **43**, 5307 (1991); J.E. Mooij, B.J. van Wees, L.J. Geerligs, M. Peters, R. Fazio, and G. Schön, *Phys. Rev. Lett.* **65**, 645 (1990).
- [12] M.-C. Cha, M.P.A. Fisher, S.M. Girvin, M. Wallin, and A.P. Young, *Phys. Rev. B* **44**, 6883 (1991).
- [13] N. Goldenfeld, *Lectures on Phase Transitions and the Renormalization Group* (Addison-Wesley, 1992), p. 44.
- [14] H.S.J. van der Zant, L.J. Geerligs, and J.E. Mooij, *Europhys. Lett.* **19**, 541 (1992).
- [15] A. Kanda and S. Kobayashi, *J. Phys. Soc. Jpn.* **64**, 3172 (1995); A. Kanda, S. Katsumoto, and S. Kobayashi, *ibid.* **63**, 4306 (1994); R. Yagi, T. Yamaguchi, H. Kazawa, and S. Kobayashi, *Czech. J. Phys.* **46**, Suppl. S2, 693 (1996).
- [16] C.J. Lobb, D.W. Abraham, and M. Tinkham, *Phys. Rev. B* **27**, 150 (1983).
- [17] J.P. Straley and G.M. Barnett, *Phys. Rev. B* **48**, 3309 (1993).
- [18] A.A. Odintsov, *Phys. Rev. B* **54**, 1228 (1996).
- [19] J. Lee, *Phys. Rev. Lett.* **71**, 211 (1993); J. Lee and M.Y. Choi, *Phys. Rev. E* **50**, R651 (1994).
- [20] M.Y. Choi and S. Doniach, *Phys. Rev. B* **31**, 4516 (1985).
- [21] P. Bak, *Rep. Prog. Phys.* **45**, 587 (1982).
- [22] R. Giachetti and V. Tognetti, *Phys. Rev. Lett.* **55**, 912 (1985); R.P. Feynman and H. Kleinert, *Phys. Rev. A* **34**, 5080 (1986).
- [23] S. Kim and M.Y. Choi, *Phys. Rev. B* **41**, 111 (1990); **42**, 80 (1990).
- [24] R.P. Feynman and A.R. Hibbs, *Quantum Mechanics and Path Integrals* (McGraw-Hill, New York, 1965).
- [25] G. Schön and A.D. Zaikin, *Phys. Rep.* **198**, 237 (1990).
- [26] See, e.g., S. Oh, S. Lee, and K.-C. Lee, *J. Korean Phys. Soc.* **27**, 365 (1994) and references therein.
- [27] D.R. Nelson and J.M. Kosterlitz, *Phys. Rev. Lett.* **39**, 1201 (1977).

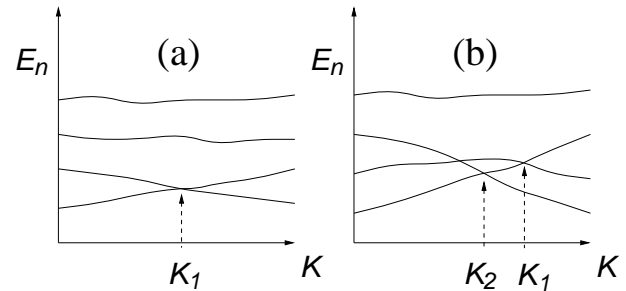


FIG. 1. Schematic diagram of the energy levels E_n versus the control parameter K . In (a) the crossing point K_1 of the ground state and the first excited state corresponds to the transition point. In (b), on the other hand, the true transition point is given by K_2 , at which the ground state meets the second excited state.

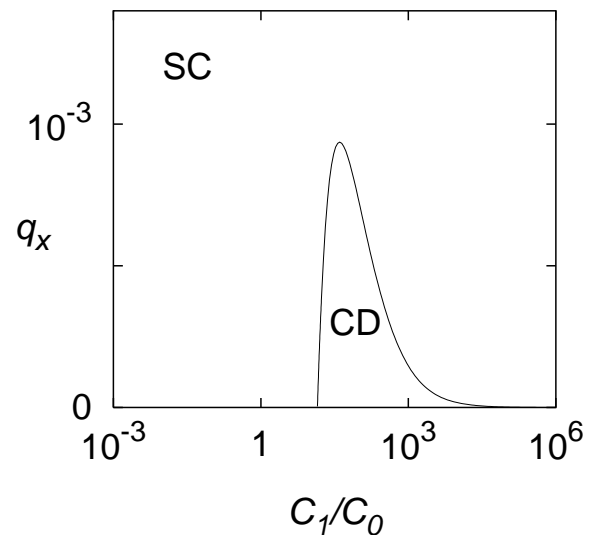


FIG. 2. Boundary for the first excited state when $\langle q_i \rangle = 0$. In the region enclosed by the curve the creation of a charge dipole (CD) at one bond gives the lowest excitation, and the creation of a single charge (SC) at one site is the lowest excitation in the region outside the curve. For $C_1/C_0 < 14.116$ the lowest excitation is SC irrespective of q_x , and in the nearest-neighbor charging limit ($C_0 = 0$) the lowest excitation is CD for $q_x = 0$ and SC for $q_x \neq 0$, respectively.

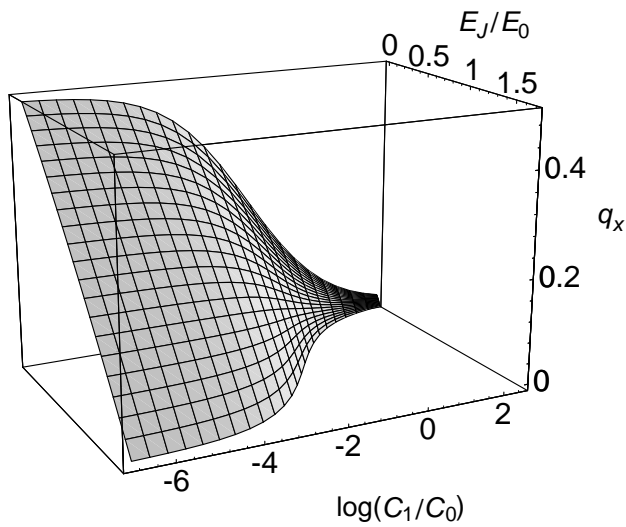


FIG. 3. Zero-temperature phase diagram for $\langle q_i \rangle = 0$. The system is insulating in the region below the surface, which shrinks monotonically as C_1/C_0 is increased.

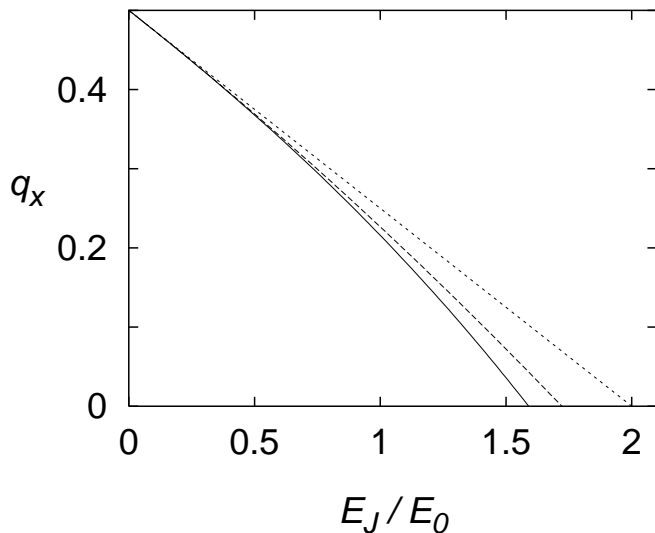


FIG. 4. Zero-temperature phase boundaries for $\langle q_i \rangle = 0$ in the self-charging limit, computed via the perturbation expansion up to $O(E_J^n)$. The dotted line, the dashed line, and the solid line correspond to the first-order ($n = 1$), the second-order ($n = 2$), and the third-order ($n = 3$) calculations, respectively.

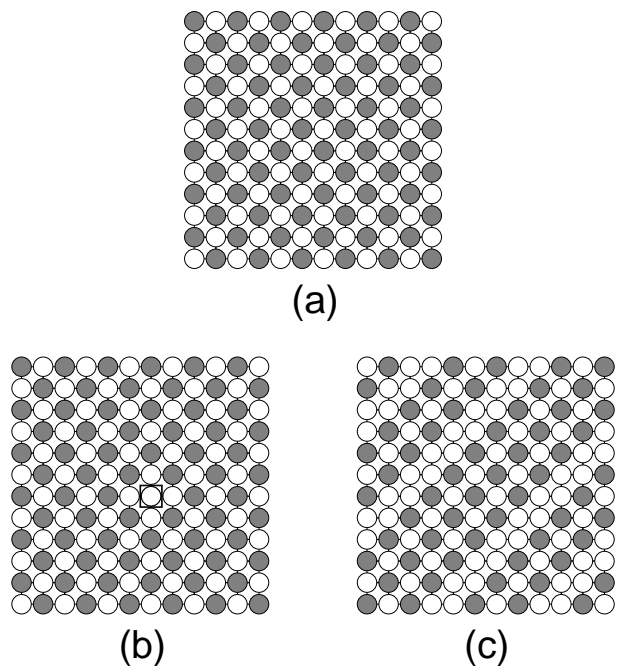


FIG. 5. (a) The commensurate charge configuration with $\langle q_i \rangle = 1/2$ at zero temperature, where the empty and the filled circles denote the vacant ($q_i = 0$) and the occupied (by single positive charges; $q_i = 1$) sites, respectively. This commensurate state is found to be destroyed by a single negative charge excitation ($q_e = -1$) for $C_1/C_0 = 1.0$ and 5.0 , as shown in (b), where the location of the point defect is indicated by a small square. When $C_1/C_0 = 0.1$, on the other hand, the lowest excitation is found to have the configuration (c), which has $q_e = -12$.

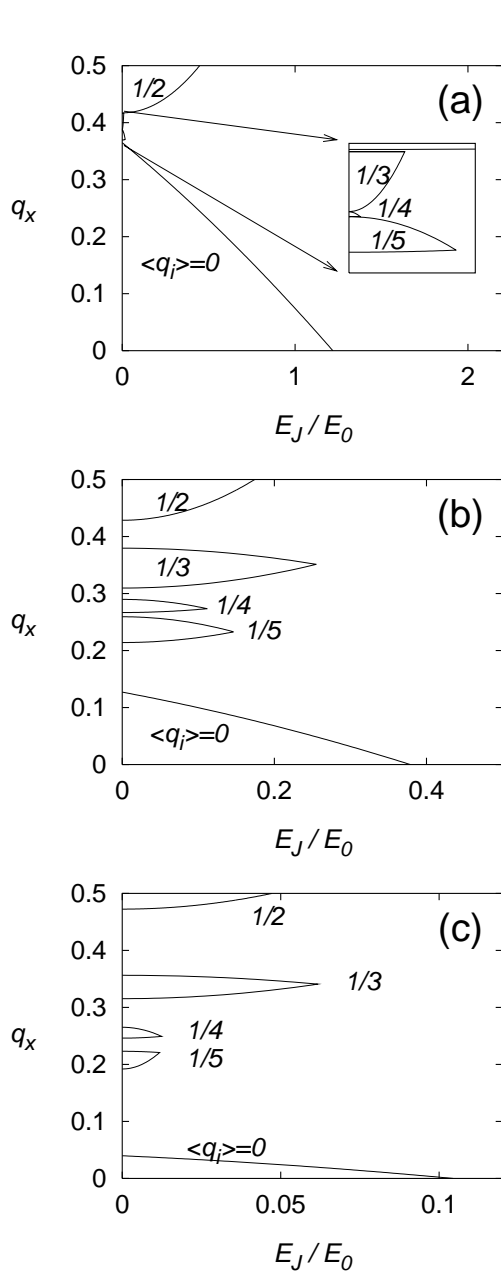


FIG. 6. The zero-temperature phase boundaries for $C_1/C_0 =$ (a) 0.1, (b) 1.0, and (c) 5.0, obtained via the second-order perturbation expansion, with the help of the simulated annealing method to find the charge configuration. Various lobe-like structures, inside of which the array is in the insulating phase, are found in both the 10×10 and the 12×12 array. As we increase the array size, additional insulating lobes are expected to be observed. As C_1/C_0 is increased, the insulating lobes become narrower, with the central position approaching $\langle q_i \rangle = q_x$. In the inset of (a), the insulating lobes with $\langle q_i \rangle = 1/3, 1/4,$ and $1/5$ are shown.

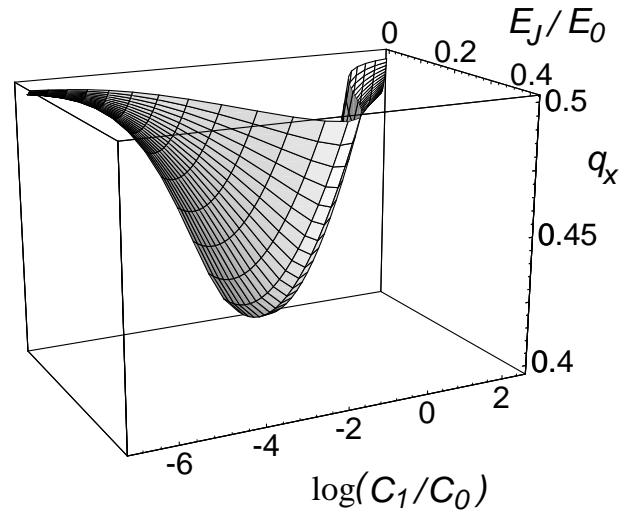


FIG. 7. Zero-temperature phase diagram for $\langle q_i \rangle = 1/2$, where only single negative charge excitation ($q_e = -1$) has been considered. In the region above the surface, charges form a 2×2 superlattice, as shown in Fig. 5 (a), leading to the insulating phase. As C_1/C_0 is increased, the insulating region expands at first (for $C_1/C_0 \lesssim 0.1$) and then shrinks.

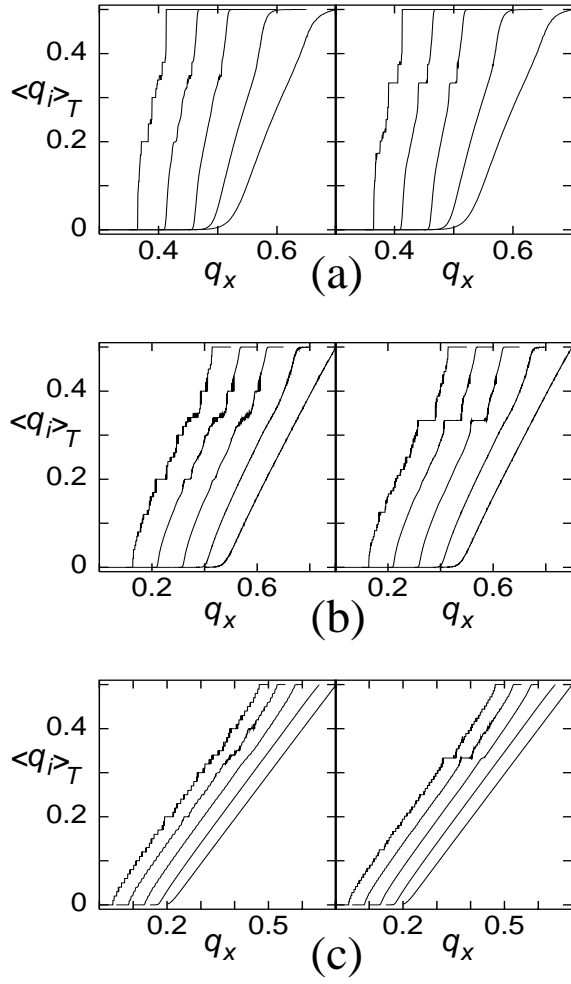


FIG. 8. Monte Carlo results of $\langle q_i \rangle_T$ as functions of q_x for arrays of sizes $L = 10$ (left) and 12 (right) with $E_J = 0$ and $C_1/C_0 =$ (a) 0.1 , (b) 1.0 , and (c) 5.0 . From the left to the right, the curves correspond to temperatures $T = 0.0, 0.006, 0.01, 0.05$, and 0.1 in (a), $T = 0.0, 0.01, 0.014, 0.04$, and 0.1 in (b), and $T = 0.0, 0.004, 0.008, 0.02$, and 0.05 in (c), respectively. Here the temperature has been measured in units of E_0/k_B , and all the curves have been shifted in the horizontal direction for clarity. More steps are expected to be observed in systems of larger sizes.

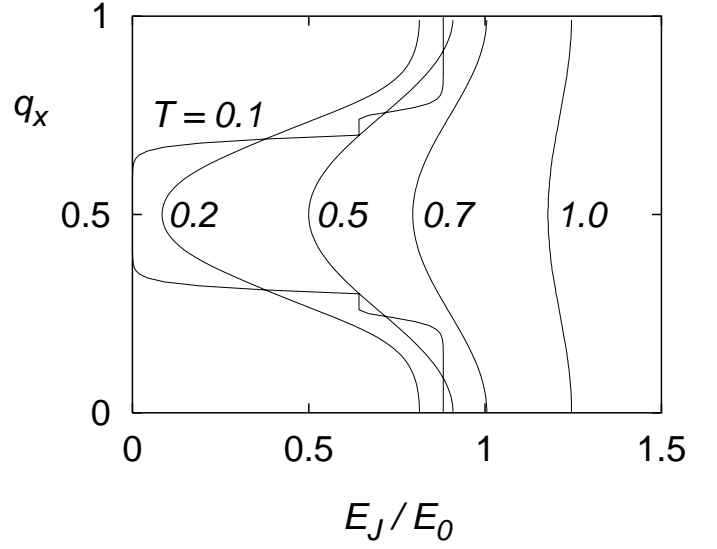


FIG. 9. Phase diagrams in the self-charging limit ($C_1 = 0$) at temperatures $T = 0.1, 0.2, 0.5, 0.7$, and 1.0 . Superconducting region (the right-hand side of each curve) is shown to expand as q_x is increased. Reentrant behavior is observed at $q_x = 0$.

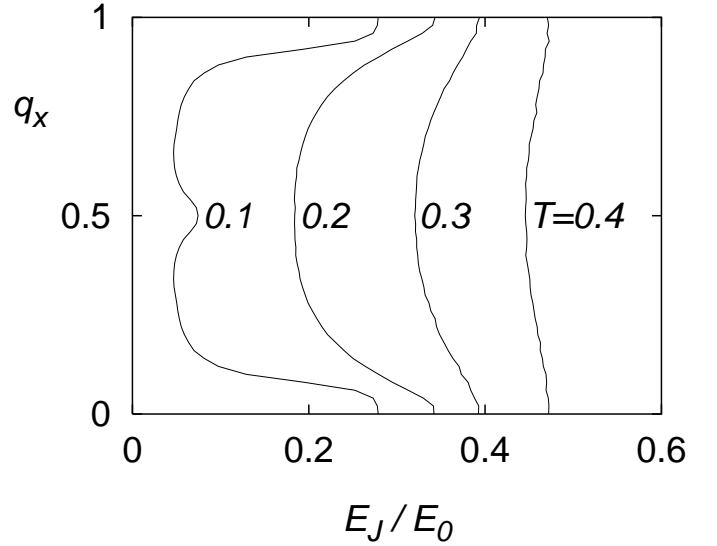


FIG. 10. Phase diagrams for $C_1/C_0 = 1.0$ at temperatures $T = 0.1, 0.2, 0.3$, and 0.4 . At $T = 0.1$, there exists a lobe-like structure near $q_x = 0.5$.

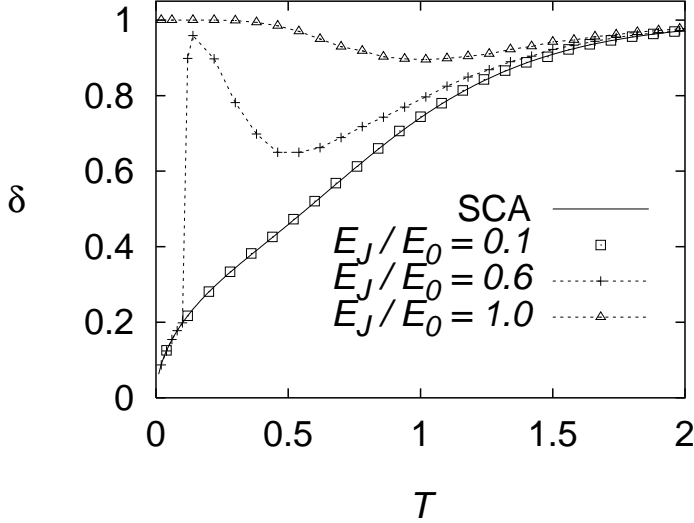


FIG. 11. Monte Carlo results of $\delta \equiv \langle \delta_{n_i, n_j} \rangle$ for $E_J/E_0 = 0.1, 0.6,$ and 1.0 , at $q_x = 0$ in the self-charging limit ($C_1 = 0$). Results from the self-consistent approximation (SCA), which are independent of E_J/E_0 , are also shown by the solid line. When the temperature is sufficiently high, the SCA is shown to give reliable results; at low temperatures, SCA results are in agreement with the MC results only for sufficiently small E_J/E_0 . Dotted lines are merely guides to the eye.

TABLE I. Values of q_e in the lowest excited states of the arrays with size (a) $L = 10$ and (b) $L = 12$. It is shown that $|q_e|$ tends to decrease as C_1 is increased.

(a) $L = 10$

$\langle q_i \rangle$	$C_1/C_0 = 0.1$	$C_1/C_0 = 1.0$	$C_1/C_0 = 5.0$
1/2	-10	-1	-1
1/5	-3, 4	-3, 3	-1, 1

(b) $L = 12$

$\langle q_i \rangle$	$C_1/C_0 = 0.1$	$C_1/C_0 = 1.0$	$C_1/C_0 = 5.0$
1/2	-12	-1	-1
1/3	-8, 12	-4, 6	-2, 2
1/4	-4, 4	-4, 3	-2, 1

TABLE II. Step width for $\langle q_i \rangle = 0, 1/3,$ and $1/2$, in the $L = 12$ array at zero temperature, obtained from the data in Fig. 8. The numbers in parentheses denote the maximum error in the last digits.

$\langle q_i \rangle$	$C_1/C_0 = 0.1$	$C_1/C_0 = 1.0$	$C_1/C_0 = 5.0$
0	$0 \leq q_x < 0.3650(5)$	$0 \leq q_x < 0.1275(5)$	$0 \leq q_x < 0.0395(5)$
1/3	$0.3900(5) < q_x < 0.4055(5)$	$0.314(1) < q_x < 0.3800(5)$	$0.317(1) < q_x < 0.356(1)$
1/2	$0.4130(5) < q_x \leq 1/2$	$0.4290(5) < q_x \leq 1/2$	$0.4725(5) < q_x \leq 1/2$

TABLE III. The critical values of E_J/E_0 at $q_x = 0$ for $C_1/C_0 = 0$ and 1.0 . The results from Monte Carlo simulations and those from Figs. 9 and 10 at temperatures $T = 0.1, 0.2,$ and 0.5 are displayed in the left and the right columns, respectively. Both results display reentrance for $C_1/C_0 = 0$. The numbers in parentheses denote the maximum error in the last digits.

T	$(E_J/E_0)_c$ for $C_1/C_0 = 0$		$(E_J/E_0)_c$ for $C_1/C_0 = 1$	
0.1	0.642(1)	0.88(1)	0.158(2)	0.28(1)
0.2	0.558(2)	0.81(1)	0.242(4)	0.34(1)
0.5	0.766(2)	0.91(1)	0.53(1)	0.57(1)